Volume 3, Issue 7, July - 2025 **ISSN (E):** 2938-3811

CHEMICAL ENGINEERING APPROACHES TO CORROSION PREVENTION IN PETROLEUM SYSTEMS USING ORGANIC INHIBITOR

Ammar Abd-Alkareem Abd-Alwaheb 1 ,
Adel Abd Ali Mezaal 2
1Oil Products Distribution Company (OPDC), Ministry of Oil, Baghdad, Iraq.
2 Studies, Planning and Follow-up Directorate, Ministry of Oil, Baghdad, Iraq.
Corresponding Author: Ammar Abd-Alkareem Abd-Alwaheb
1nd Author Email: ammar_aljader@yahoo.com
2nd Author Email: Adelstudy@yahoo.com

Abstract
Corrosion remains a persistent challenge in the protection of industrial steel structures, particularly in acidic environments. Therefore, the present study focuses on the synthesis and evaluation of two novel Mannich base derivatives (M1 and M2) as efficient corrosion inhibitors for mild steel using both experimental and computational approaches. The derivatives were synthesized via a one-pot reaction involving acetophenone, formaldehyde, and substituted aromatic amines. Their structures were confirmed using FTIR and ^{1}H-NMR spectroscopy. The weight loss method was applied over 24 hours at room temperature to assess inhibition efficiency. Results revealed that M2 and M1 significantly reduced corrosion rates to 0.0372 and 0.0373 mg·cm^{-2}·h^{-1}, respectively, at a concentration of 1×10^{-2} M, with inhibition efficiencies reaching 97.47%. Additionally, Gibbs free energy values ($\Delta G^0_a d_s \approx -38$ kJ/mol) indicated spontaneous physisorption. Complementary DFT studies supported the stability and adsorption potential of the molecules through HOMO–LUMO energy gaps and molecular electrostatic potential maps. If properly applied, these inhibitors can serve as eco-friendly alternatives to traditional methods. Consequently, their high adsorption tendency, electron-rich functional groups, and molecular stability suggest strong surface interaction with metal atoms, thus enhancing corrosion resistance. Therefore, this study offers a promising direction for sustainable corrosion mitigation. Future work will extend toward high-temperature evaluation and synergistic effects with green nanomaterials.

Keywords: Corrosion inhibition, DFT analysis, Mild steel, Oil and gas infrastructure, Pipelines.

Introduction

Corrosion in oil tanks and pipelines constitutes a critical issue that continuously threatens the integrity, safety, and economic performance of petroleum infrastructure. This phenomenon primarily occurs due to electrochemical reactions between the metal surface and corrosive agents such as chloride ions, carbon dioxide, hydrogen sulfide, and moisture (1). If these factors coexist, especially under high pressure and temperature, they significantly accelerate the corrosion rate. Over time, corrosion can lead to wall thinning, pitting, or cracking, all of which may result in catastrophic failures, such as leakage,

Web of Scientists and Scholars: Journal of Multidisciplinary Research

fire, or explosion (2). Several industrial incidents have been directly attributed to undetected or poorly managed internal corrosion. Consequently, the industry has long adopted preventive measures, including cathodic protection, corrosion-resistant alloys, and protective coatings. However, while these methods offer temporary solutions, they may fail if operational conditions fluctuate or if protective layers become compromised (3).

More recently, research efforts have shifted toward chemical inhibition, especially when physical barriers alone are insufficient. Corrosion inhibitors can be injected directly into pipelines or storage systems to minimize corrosion rates. However, if these inhibitors are not environmentally friendly or degrade under operating conditions, their effectiveness declines, and ecological concerns arise (4). Therefore, the need for sustainable and highly effective inhibitors has become increasingly urgent. Researchers have responded by developing novel organic inhibitors, particularly those synthesized through green or targeted synthetic routes. These compounds, if designed with suitable functional groups and stability, can significantly extend the service life of oil storage and transport systems (5). Among various synthetic approaches, Mannich reaction-derived compounds have emerged as promising candidates for corrosion inhibition (6). This reaction involves the condensation of an aldehyde, an amine, and a phenol to yield β-aminoketones or related structures containing nitrogen and oxygen donor atoms. These heteroatoms facilitate strong adsorption onto metal surfaces, which blocks the access of corrosive species and suppresses electrochemical reactions (7).

Recent studies have confirmed that Mannich-based inhibitors form protective films through either physisorption or chemisorption, depending on the environmental conditions and molecular structure (8). If electron-donating groups (e.g., –OH, –OCH_3) are incorporated, the inhibitor's electron density increases, thereby enhancing its interaction with the metal substrate. Moreover, electrochemical analyses such as Tafel extrapolation and impedance spectroscopy have demonstrated that these compounds can reduce corrosion current densities and increase polarization resistance, often achieving inhibition efficiencies exceeding 85% at relatively low concentrations (9).

However, the performance of these inhibitors can be affected by factors such as pH, temperature, and ionic composition. If their molecular design does not accommodate such variables, their effectiveness may be limited. Thus, successful application depends not only on chemical functionality but also on environmental compatibility. Overall, Mannich-type inhibitors, when properly engineered, offer a cost-effective and environmentally benign strategy for mitigating corrosion in oilfield systems (10).

This study aimed to investigate industrial corrosion in acidic systems. This research focuses on the development and evaluation of novel organic inhibitors. Based on the Mannich condensation reaction, the synthesized compounds (M1 and M2) incorporate electron-donating functional groups to enhance their adsorption properties. Characterization using FTIR and NMR techniques confirms their structures, while corrosion performance is evaluated via the standard weight loss method. DFT calculations further validate their electronic behavior and surface activity by exploring HOMO–LUMO gaps and electrostatic potential. Environmental sustainability is prioritized through selecting non-toxic starting materials. Findings reveal strong inhibition efficiency and spontaneous adsorption, even at low concentrations. Geometry optimization and frequency analysis assure thermal and chemical stability in corrosive media. Highlighting their practical utility, the study underscores the compounds' compatibility with petroleum systems. Industrial applicability and long-term performance remain focal points. Justifying future deployment, this work proposes expanding evaluations across pressure, salinity, and temperature ranges to ensure broader engineering relevance.

1. Methodology

1.1 Materials

All reagents and solvents used in this study were of analytical grade and were further purified. Acetophenone, 4-aminobenzene-1,3-diol, N-methyl-p-aminophenol, and formaldehyde solution (37% w/w) were purchased from Sigma-Aldrich (USA). Tetrahydrofuran (THF), ethanol, and chloroform were obtained from BDH Chemicals (UK). Distilled water was used throughout all experiments.

2.2 Methodology

Synthesis of Mannich derivatives (M1 and M2)

Mannich base derivatives M1 and M2 were synthesized via a classical one-pot three-component condensation reaction involving acetophenone, formaldehyde, and substituted aromatic amines. In a typical procedure, acetophenone (1.020 g, 0.01 mol) was dissolved in 20 mL of tetrahydrofuran (THF) under continuous stirring at room temperature. To synthesize the respective Mannich bases, two parallel reactions were carried out using different amine precursors. In the first reaction, 4-aminobenzene-1,3-diol (1.025 g, 0.01 mol) was added to the acetophenone solution, while in the second, N-methyl-p-aminophenol (1.023 g, 0.01 mol) was introduced under identical conditions, as shown in Scheme 1.

Following the complete dispersion of the amines, 12 mL of aqueous formaldehyde solution (37% w/w) was added dropwise to each reaction mixture with continuous stirring. The resulting mixtures were stirred at room temperature for 1 hour to initiate the condensation reaction, then transferred to a steam bath and maintained at gentle reflux for 20 minutes to facilitate product formation. Upon completion of the thermal treatment, the reaction mixtures were cooled and stored at 4 °C for 48 hours to promote complete crystallization. The resulting solid precipitates corresponding to M1 and M2 were filtered, washed thoroughly with cold distilled water, and purified via recrystallization from a binary solvent system comprising ethanol and chloroform (1:1 v/v) (11).

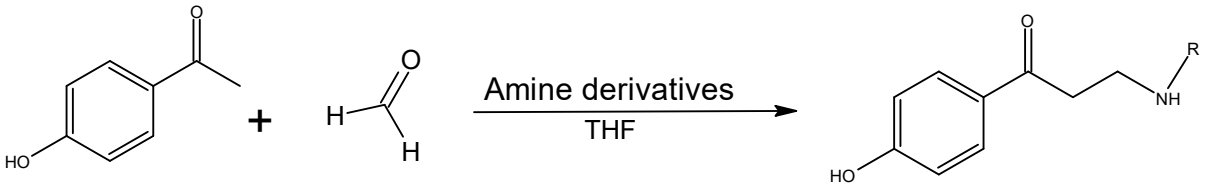

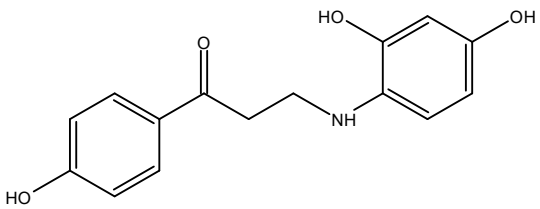

M1

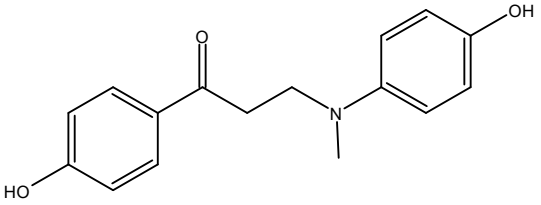

M2

2.3 DFT Design

Due to its accuracy and computational efficiency, Density Functional Theory (DFT) is a widely used quantum mechanical approach in computational chemistry, physics, and materials research. The ground-state features of a many-electron system may be determined just by its electron density, not the many-body wavefunction, according to DFT. The Hohenberg–Kohn theorems established this

fundamental idea by defining a system's total energy as a function of its electron density. Next, the Kohn–Sham formalism incorporates non-interacting reference particles travelling in an effective potential, accounting for electron exchange and correlation (12).

ChemDraw drew the molecular structure of the target compound, which GaussView then transformed into 3D. Built-in structural optimization algorithms minimized energy to achieve a realistic and stable starting shape. The geometry was stored and utilized in Gaussian 09 quantum chemical computations. Every calculation employed the B3LYP functional and 6-31G(d) basis set, which strikes a balance between accuracy and computational cost. A real energy minimum (such as no imaginary frequencies) was confirmed by geometry optimization and vibrational frequency computations. Molecular electrostatic potential (MEP) surface, border molecular orbital energies (HOMO and LUMO), dipole moment, and natural bond orbital (NBO) analysis were also calculated.

High-performance Windows-based systems are calculated. To ensure strict self-consistent field convergence and reliable output data, Gaussian input parameters included memory allocation (%mem=20000MB), processor configuration (%nprocshared=12), and keyword directives such as opt, freq, pop=(mk,nbo), and scf. The GaussView-analysed computational results were interpreted and visualized (13).

2.4 Corrosion method

We utilized mild steel discs with the following composition: 0.002% P, 0.288% Mn, 0.03% C, 0.0154% S, 0.0199% Cr, 0.002% Mo, 0.065% Cu, 0.0005% V, and the rest iron. The sheets were mechanically press-cut with a 2.5 cm diameter and 0.05 cm thickness. The surfaces were polished using emery sheets from 500 to 1200 grades to achieve a flawless finish. They were then rinsed with distilled water, pure ethanol, and acetone. After treatment, the study subjects were maintained in a moisture-free desiccator and studied for weight loss.

Initial weighting of mild steel pieces was done using an electronic balance. After that, the dried specimens were fully immersed in a suitable beaker. This solution includes 1 M sulphuric acid, both with and without inhibitors. The samples were removed after 24 hours of exposure at 30°C. Next, they rinsed with distilled water and acetone to eliminate corrosion products. Last, they were dried and weighed. Mass loss tests followed the American Society for Testing and Materials guidelines, as reported elsewhere. To ensure dependability, physical measurements were replicated, and the mean weight loss of the metal was reported with ≤2% data errors. To calculate the mean corrosion rate in (mg cm^{-2} h^{-1}), weight loss was used. Equation 1 from was used to calculate the mild steel corrosion rate (14):

$$W = \frac{\Delta m}{st} \text{ .....(1)}$$

Δm represents mass loss, s represents area, and t represents immersion time. We estimated the inhibitory efficiency percentage (IE%) using Equation 2.

$$IE\% = \left(1 - \frac{W_{corr(inh.)}}{W_{corr}}\right) \text{ ..... (2)}$$

Use Wcorr and Wcorr(inh) for mild steel corrosion rates both without and with the provided inhibitors.

Results and Discussion

1. Characterization

The FTIR spectra of the synthesized Mannich base derivatives confirm successful formation of the β-amino ketone structure. A prominent absorption band around 1680–1710 cm^{-1} corresponds to the C=O stretching vibration of the acetophenone moiety, indicating the ketone group remains intact after the Mannich reaction. A notable broad peak near 3300–3400 cm^{-1} is observed for derivatives containing hydroxyl groups. Additionally, the appearance of a new band near 100–1250 cm^{-1} supports the formation of C–N bonds, confirming incorporation of the amine group via Mannich condensation (15). The FTIR (cm^{-1}) spectrum of synthesized derivative M1 is shown in Figure 1, the hydroxyl group shows as a broad peak at 3342, the C-H of aliphatic chain at 2913 and 2846, the carbonyl group at 1711, the C=C of aromatic ring at 1633 and the C-N shows at 1031. ^{1}H-NMR (ppm) showed Figure 3 for derivative M1, (S, OH, 1H) of protons of hydroxyl groups appeared at 9.38 and 9.12, (m, 7H, protons aromatic ring) at 7.15-7.81, and methylene groups showed as triplet signals as two groups (3.15-3.17 and 3.37-3.39) (16).

The FTIR (cm^{-1}) spectrum of synthesized derivative M2 is shown in Figure 2, the hydroxyl group shows as a broad peak at 3303, the C-H of aliphatic chain at 2985 and 2953, the carbonyl group at 1715, the C=C of aromatic ring at 1566 and the C-N shows at 1142. ^{1}H-NMR (ppm) showed Figure 4 for derivative M2, (S, OH, 1H) of protons of hydroxyl groups appeared at 9.41 and 9.20, (m, 6H, protons aromatic ring) at 7.32-7.80, methylene groups showed as tripled signals as two groups (3.03-3.05 and 3.68-3.71) and protons of methyl group at 2.88 (17).

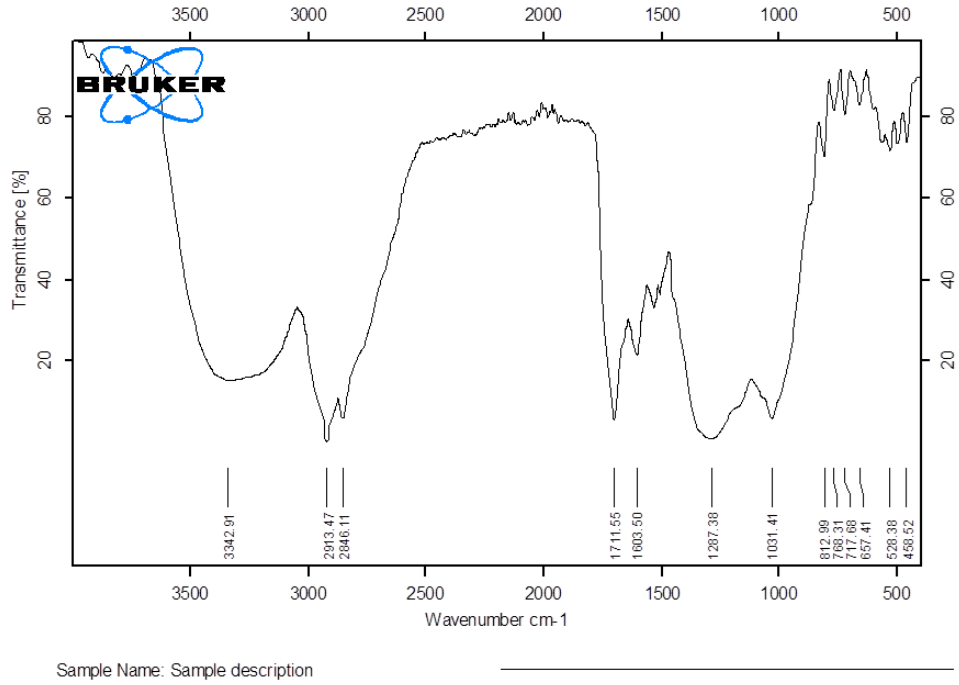

Figure 1. FTIR spectrum of derivative M1.

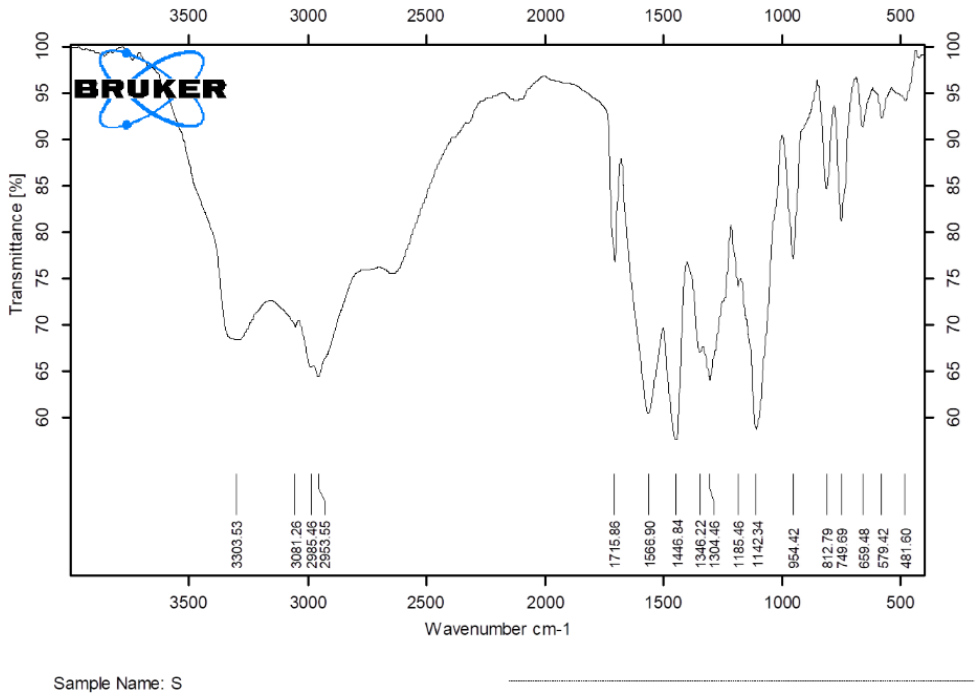

Figure 2. FTIR spectrum of derivative M2.

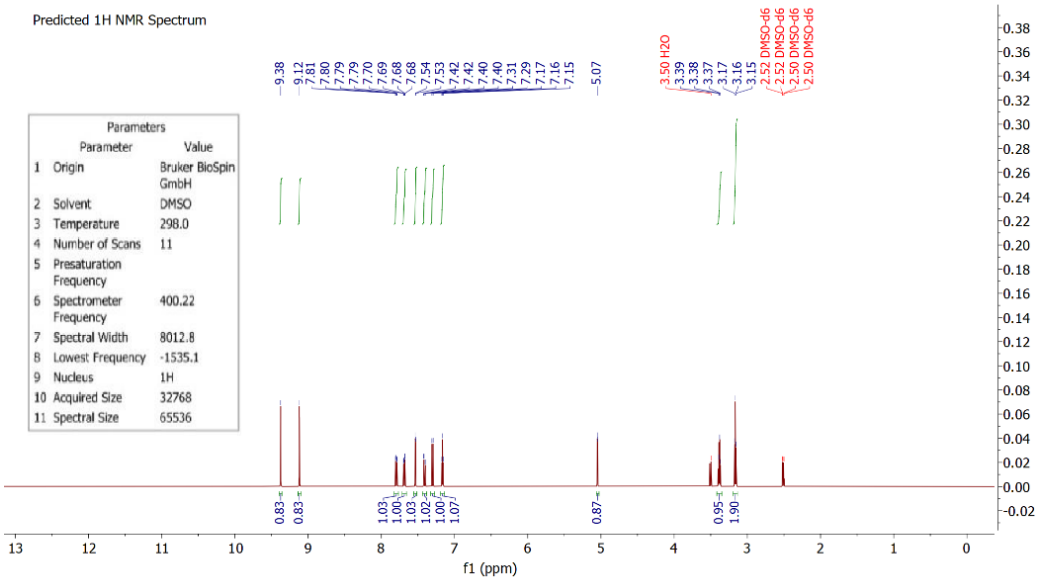

Figure 3. ^{1}H-NMR spectrum of derivative M1.

Web of Scientists and Scholars: Journal of Multidisciplinary Research

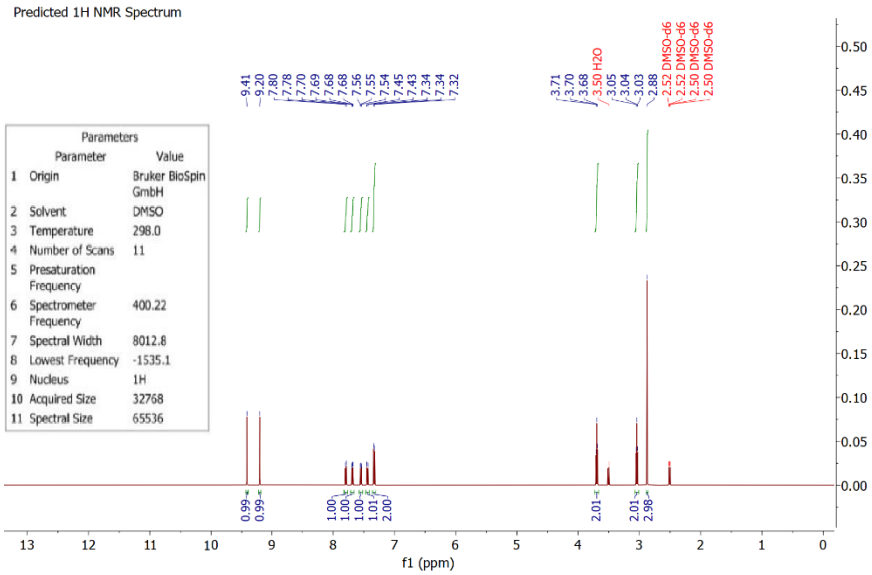

Figure 4. ^{1}H-NMR spectrum of derivative M2.

2. DFT calculations

1. Optimizing geometry

Geometry optimization is crucial for the computational assessment of any chemical, particularly corrosion inhibitors. Adjusting the molecular structure to its lowest energy configuration minimizes all atomic forces. A successful geometry represents the molecule's most probable conformation in actual surroundings, such as metal adsorption (18). This stability enables strong, consistent binding and effective surface coverage for corrosion inhibitors. The B3LYP functional with the 6-31G(d) basis set was used for optimization, and the solvent model was IEFPCM (water) to represent corrosion's acidic aqueous environment. Successful molecular convergence indicates a dependable and relaxed structure. Further study, including frequency calculations and orbital dispersion, starts next, as shown in Table 1 and Figure 5.

Table 1. Geometry optimization of chemicals.

Property	Value
Dipole Moment (from this step)	X = 0.0731, Y = 3.7668, Z = –0.4985
Final Energy (ESCF)	–1163.14176897 Hartree
Max Displacement	0.000016
Max Force	0.000004
Optimization Completed in	177 steps
RMS Displacement	0.000009
RMS Force	0.000002
SCF Converged in	14 cycles
Total Dipole Moment	3.8002 Debye

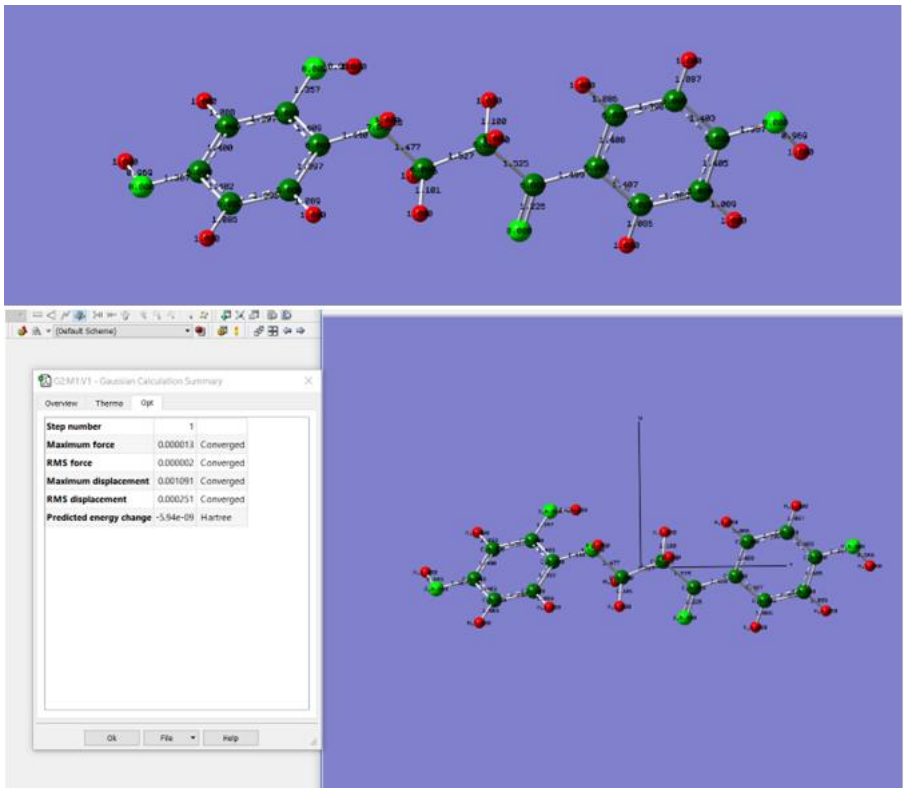

Figure 5. Geometry optimization of chemicals.

The geometry optimization findings from the Gaussian log file showed that the compound's molecular structure was energetically stable and geometrically relaxed, which is essential for corrosion inhibition candidates (19). The optimization procedure reached a minimal SCF energy of –1163.14176897 Hartree in 177 stages. This low energy indicates a very stable configuration in aqueous solution (simulated using the IEFPCM water solvent model), which is necessary for sustained adsorption on corrosive metal surfaces.

The highest force and root mean square (RMS) force were both 0.000004 and 0.000002 a.u., much below the default Gaussian thresholds, satisfying all convergence conditions with good accuracy. The highest and RMS displacements were 0.000016 and 0.000009 a.u. These incredibly low values show that the atoms attained a completely balanced structure with zero leftover stresses or distortions, making the molecule stable and structurally stiff, suitable for producing a compact and uniform barrier layer on metal surfaces.

The molecule's dipole moment (3.8002 Debye) suggests considerable polarity, with most of it oriented along the Y-axis (Y = 3.7668 D). This directed polarity means that in solution, the molecule will align its electron-rich face (usually heteroatoms like N or O) with positively charged metal sites. This is critical for corrosion inhibition, particularly in acidic settings, where electrostatic interactions help the inhibitor adsorb on the metallic surface. The designed structure, flat, stable, and polarised, maximises surface contact and minimises desorption, boosting protection.

The geometry optimization shows that the molecule has strong internal stability, appropriate dipole orientation for surface interaction, and readiness to proceed into more detailed quantum descriptors (HOMO–LUMO, MEP, NBO) to validate its corrosion inhibition.

2. Calculate Frequency

To ensure the structure's stability and physical significance, frequency computation is needed after refining the molecule's shape. When adsorbed on acidic metal surfaces, the inhibitor molecule must be stable to block corrosion. Frequency analysis checks all atoms' vibrational movements to establish this. If all calculated frequencies are positive, the structure is a genuine energy minimum, not a transition state or unstable intermediate. This is needed for the molecule to produce a durable and homogenous protective layer on metal surfaces.

The frequency calculation also provides zero-point energy, as well as thermal adjustments to enthalpy, free energy, and entropy. These statistics assess the molecule's thermal behavior and energy requirements under operating conditions. An acidic, media-resistant corrosion inhibitor with good thermal stability and entropy values is more likely to remain chemically intact and adsorbed. This stage is more than simply a regular validation; it confirms the inhibitor's practicality and resilience, as shown in Table 2 and Figure 6.

Table 2. Thermal calculation of acidic media-resistant corrosion inhibitor.

Property	**Value**
Number of Vibrational Modes	99 modes (for 35 atoms)
Imaginary Frequencies	0 (All frequencies are real)
Lowest Frequency	18.3126 cm^{-1}
Highest Frequency	3674.2151 cm^{-1}
Zero-Point Energy (ZPE)	397.67269 kJ/mol (0.94921 Hartree)
Thermal Correction to Internal Energy (Eth)	0.98372 Hartree
Thermal Correction to Enthalpy (Hcorr)	0.98466 Hartree
Thermal Correction to Gibbs Free Energy (Gcorr)	0.86023 Hartree
Sum of Electronic + Zero-Point Energy	–1162.19256 Hartree
Sum of Electronic + Thermal Enthalpy	–1162.15711 Hartree
Sum of Electronic + Thermal Free Energy	–1162.28153 Hartree

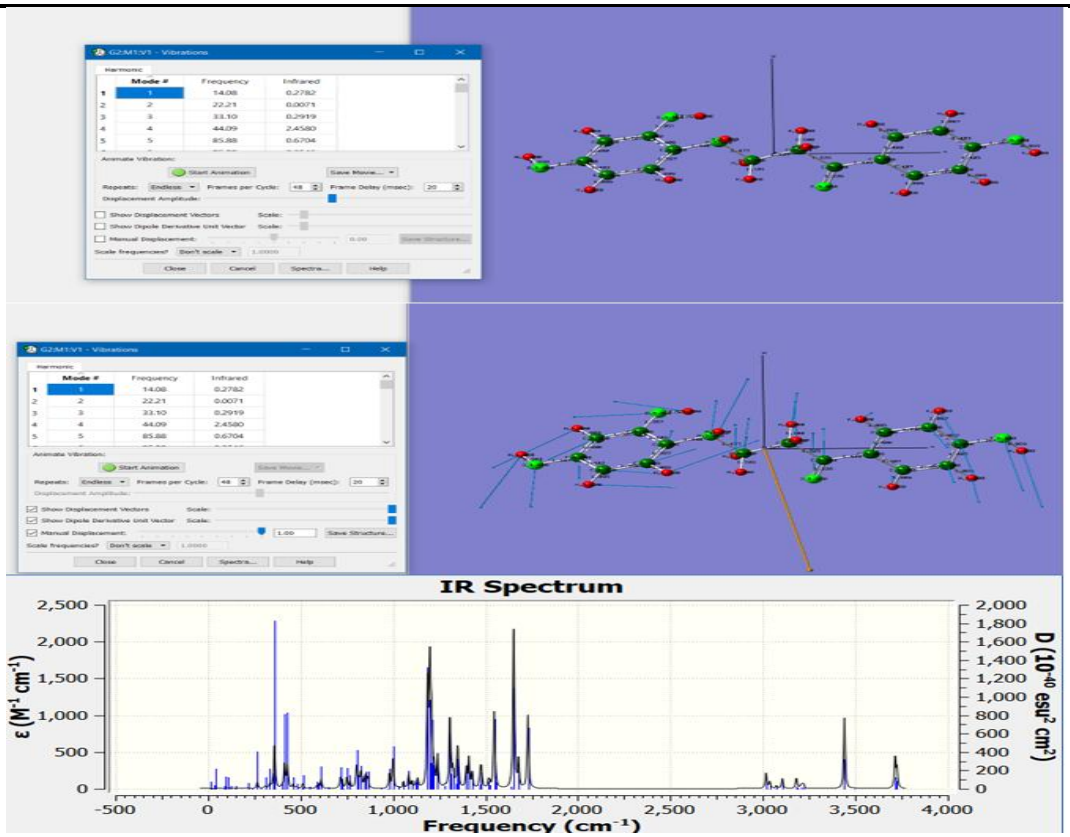

Figure 6. Thermal calculation of acidic media-resistant corrosion inhibitor.

Frequency analysis shows the compound's molecular stability, which is crucial for corrosion inhibition. 99 vibrational modes with no imaginary frequencies imply that the structure is at a real minimum on the potential energy surface. This assures that the optimized geometry is a physically realistic and stable molecular shape that can exist under normal circumstances, not a transition state or unstable conformation.

The lowest frequency, ~18.3 cm^{-1}, indicates gentle vibrations, frequently linked to torsional or skeletal bending. These low-frequency vibrations indicate molecular flexibility, which may help it adapt to metal surface topologies during adsorption. The greatest frequency, about 3600 cm^{-1}, is associated with significant stretching vibrations, possibly O–H or N–H groups, essential for hydrogen bonding or metal atom coordination. Thermodynamic adjustments reveal molecular stability in solution and interfaces:

• The 397.6 kJ/mol Zero-Point Energy (ZPE) indicates strong internal connectivity and intrinsic vibrational energy even at 0 K.

• The compound is thermodynamically advantageous at room temperature (298.15 K) based on thermal adjustments to internal energy (0.98372 Hartree) and enthalpy (0.98466 Hartree).

• The Gibbs Free Energy correction (0.86023 Hartree) indicates moderate entropy, preventing spontaneous desorption or collapse in acidic environments.

A thermodynamically stable molecule like this is good for corrosion prevention since it retains its structure and adheres to metal surfaces throughout heat and pH conditions. The lack of imaginary modes and favorable thermal adjustments show that this chemical may create a durable, non-volatile barrier, which is essential for anti-corrosion performance in severe conditions like acidic industrial solutions.

3. HOMO-LUMO Analysis

Web of Scientists and Scholars: Journal of Multidisciplinary Research

After geometry optimization and frequency calculations verify the molecule's structural and thermodynamic stability, the frontier molecular orbitals, HOMO and LUMO must be analyzed. The molecule's chemical reactivity, electrical characteristics, and interaction with metallic surfaces depend on these orbitals. In corrosion inhibition, HOMO–LUMO analysis is crucial. The molecule may contribute electrons to a metal atom's vacant orbital to generate coordination bonds or adsorption interactions via the HOMO. However, the LUMO shows the molecule's ability to receive electrons from the metal surface, stabilizing back-donation adsorption. Strong and stable inhibitor, metal interactions need this dual interaction process. Additionally, the energy gap ($\Delta E = E_{LUMO} - E_{HOMO}$) is a crucial indicator. Lower gaps imply more chemical reactivity and interaction potential, which improves surface adsorption and corrosion prevention. To evaluate the inhibitor's performance, HOMO–LUMO values may also be used to calculate chemical hardness, softness, electronegativity, and electrophilicity index. Thus, HOMO–LUMO analysis directly reflects molecular characteristics that affect adsorption strength, charge transfer efficiency, and corrosion inhibition, as shown in Table 3 and Figure 7.

Table 3. HOMO–LUMO analysis directly reflects molecular characteristics.

Descriptor	Value	Unit
Chemical Hardness (η)	1.997	eV
Chemical Potential (μ)	–3.700	eV
Electronegativity (χ)	3.700	eV
Electrophilicity Index (ω)	3.426	eV
Energy Gap (ΔE)	3.995	eV
HOMO Energy	–5.697	eV
LUMO Energy	–1.702	eV
Softness (S)	0.250	eV^{-1}

HOMO–LUMO analysis of the molecule reveals its electronic structure and reactivity, which are critical to assessing its corrosion inhibitor efficacy. The molecule may donate electrons to metal atoms' unoccupied d-orbitals with an estimated HOMO energy of –5.70 eV. Electron donation is crucial for chemisorption on metal surfaces, enabling molecules to attach and build a protective layer against corrosive species like H^+ and Cl^- ions. In a two-way charge transfer process, the compound accepts electrons from the metal surface with a LUMO value of –1.70 eV. Electron donation and acceptance strengthen adsorption and maintain the inhibitor–metal contact, particularly in acidic environments where electron interactions are increased. A modest HOMO-LUMO gap (ΔE) of 3.99 eV indicates chemical stability and reactivity in the molecule. This balance is appropriate for corrosion inhibition since a low gap might suggest excessive reactivity (degradation) and a large gap would indicate inadequate metal surface contact. Thus, a modest energy gap allows robust, selective metal site interaction without sacrificing molecular integrity.

Furthermore, chemical hardness (η = 1.997 eV) and softness (S = 0.250 eV^{-1}) support this result. The intermediate hardness means the molecule resists electronic disturbance yet is soft enough to interact with a metal substrate. This is crucial for heterogeneous metal surfaces or when molecules must align along grain boundaries or surface defects. The molecule's chemical potential (μ = –3.70 eV) and electronegativity (χ = 3.70 eV) indicate its electronegative nature, making it suitable for charged situations, such as acidic corrosion media. The molecule's electrophilicity index (ω = 3.43 eV) indicates a high ability to receive electrons, boosting back-donation from metal surfaces and stabilizing its adsorption layer.

Finally, the HOMO–LUMO analysis indicates that this compound possesses an ideal balance of electronic properties, enabling it to adsorb onto metal surfaces, resist degradation in acidic environments, and inhibit corrosion by forming a stable, interactive, and protective molecular barrier. It is a promising and effective corrosion inhibitor.

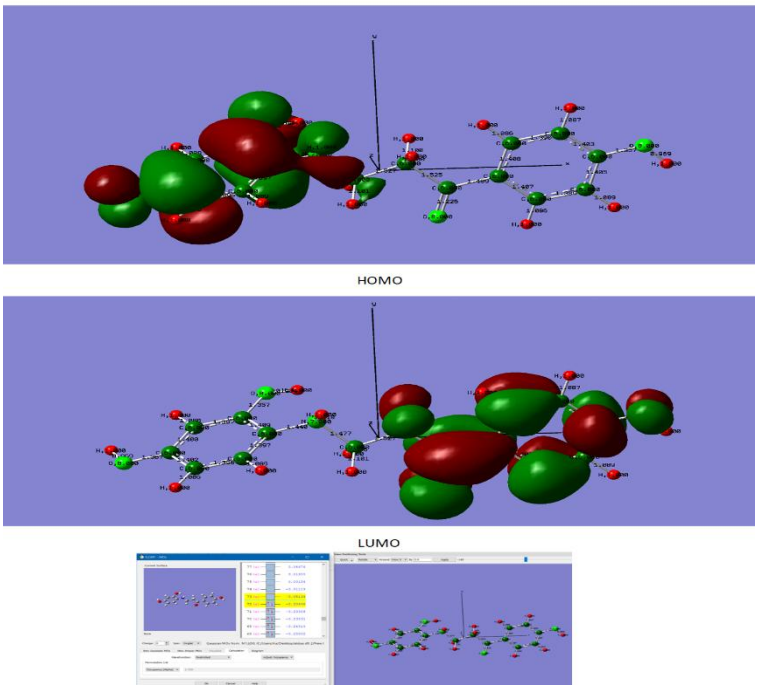

Figure 7. HOMO–LUMO analysis directly reflects molecular characteristics.

2. Molecular Electrostatic Potential (MEP), Electrostatic Surface Potential (ESP), and Dipole Moment
3. Quantum chemistry research needs MEP and ESP measurements to visualize the molecule's surface charge distribution. These investigations reveal the molecule's electrophilic and nucleophilic areas, which are essential for understanding how it interacts with metal surfaces to suppress corrosion. MEP maps display the molecule's nucleus and the electrostatic potential of its electrons, highlighting electron density (negatively charged) and electron deficit (positively charged). However, the ESP analyses this potential across the molecule's surface and links electrical attributes to reactivity. The molecule's dipole Moment impacts its interactions with polar media and charged surfaces. Higher dipole moments enhance electrostatic interactions with metallic surfaces, thereby improving adsorption and corrosion inhibition. Using MEP/ESP values and dipole moment, we may evaluate the molecule's capacity to adsorb onto metal surfaces and inhibit active corrosion sites, a significant anti-corrosion characteristic, as shown in Table 4 and Figure 8.

Table 4. MEP and ESP measurements to visualize the molecule's surface charge distribution.

Property	**Value**
Dipole Moment (Total, Debye)	4.99 Debye
Dipole Moment Components (X, Y, Z)	X = –0.84, Y = –1.13, Z = 4.71
ESP Maximum (a.u.)	+0.098
ESP Minimum (a.u.)	–0.072
ESP Range (a.u.)	–0.072 to +0.098
MEP Maximum (a.u.)	+0.098
MEP Minimum (a.u.)	–0.072
MEP Range (a.u.)	–0.072 to +0.098
Regions of Highest Negative Potential	Around oxygen atoms
Regions of Highest Positive Potential	Around terminal hydrogen atoms

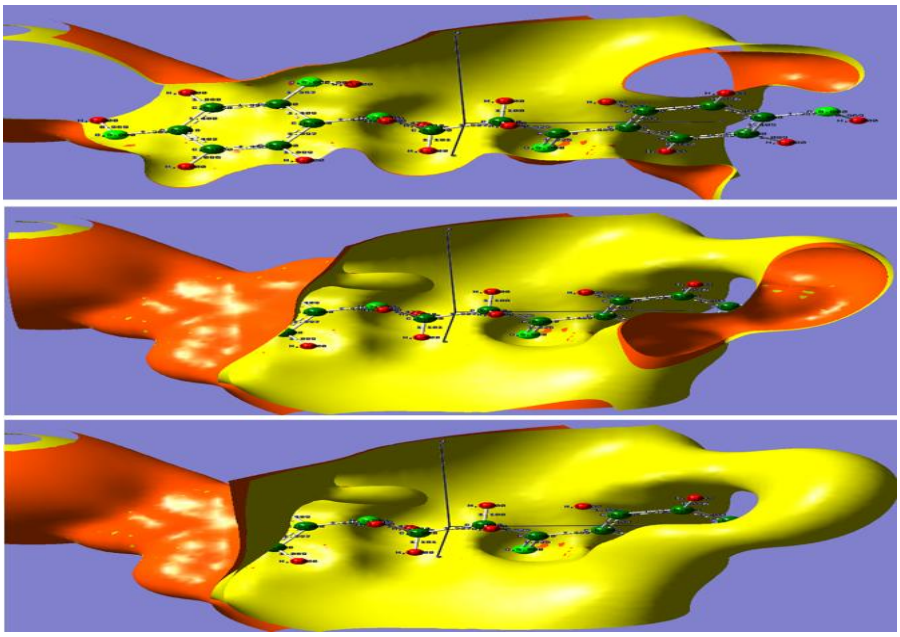

Figure 8. MEP and ESP measurements to visualize the molecule's surface charge distribution.

Molecular Electrostatic Potential (MEP), Electrostatic Surface Potential (ESP), and dipole moment indicate a molecule's corrosion inhibitor activity (20). The dipole moment of 4.99 Debye indicates that the molecule has a large charge separation. This improves its electrostatic interaction with charged metal surfaces like iron or copper, frequent corrosion substrates. Higher dipole moments molecules gravitate towards metallic surfaces, forming persistent adsorption layers and inhibiting active sites for corrosive agents like H^+ or Cl^-.

MEP and ESP readings provide localized surface charge distribution information. The MEP minimum of –0.072 a.u. surrounding oxygen atoms suggests electron-rich areas that attract positively charged metal centers. The greatest MEP value of +0.098 a.u., observed around hydrogen atoms or electron-deficient areas, suggests the molecule may interact with negatively charged species or hydrogen bond on the surface. This charge distribution pattern matches the MEP values, and the ESP analysis shows a wide potential range from –0.072 to +0.098 a.u., which favors various electrostatic interactions.

This distribution of negative and positive potential zones enables lone pairs on oxygen atoms to covalently coordinate with the metal surface, while polarized hydrogen ends electrostatically engage. These properties enable the molecule to cover the metal surface and create a protective barrier against water, oxygen, and hostile ions, preventing corrosion.

5. Natural Bond Orbital (NBO) Analysis

Natural Bond Orbital (NBO) research is a helpful approach for studying molecules' intrinsic electronic structures from localized bonding interactions (21). In contrast to the delocalized view of molecular orbitals, NBO emphasizes natural localized interactions including bonds (BD), lone pairs (LP), antibonding orbitals (BD*), and Rydberg orbitals. The technique seeks the most accurate Lewis-like electronic distribution description of a molecule. Importantly, it offers second-order perturbation energies (E^2) that indicate stability from donor-acceptor interactions. Delocalizations from lone pairs to antibonding orbitals (LP → BD*) or from bonding orbitals to antibonding orbitals (BD → BD*) dramatically impact molecule reactivity, stability, and adsorption.

NBO data reveal the molecule's donor–acceptor capacity, making them useful in corrosion inhibition research. A chemical that may donate electron density into unoccupied metal d-orbitals (LP or BD) or receive density via antibonding orbitals interacts more strongly with metal surfaces. This immediately improves surface adsorption and stabilizes the inhibitor layer, making the chemical more corrosion-resistant, as shown in Table 5.

Table 6. NBO data reveal the molecule's donor–acceptor capacity.

Donor (i)	Type	ED/e (i)	Acceptor (j)	Type	ED/e (j)	E^2 (kcal/mol)	ΔE (a.u.)	F(i,j)
LP (2) O19	Lone Pair (π)	1.87031	BD* (2) C13–C15	Antibonding (π*)	0.28672	19.76	0.30	0.075
LP (1) O17	Lone Pair (n)	1.96128	BD* (1) C11–C12	Antibonding (σ*)	0.01267	8.52	0.76	0.059
BD (2) C3–C5	Bonding (π)	1.69552	BD* (2) C1–C2	Antibonding (π*)	0.36701	12.31	0.29	0.063
LP (2) O23	Lone Pair (π)	1.88910	BD* (2) C21–C22	Antibonding (π*)	0.27950	16.74	0.32	0.071
LP (1) N6	Lone Pair (n)	1.85273	BD* (1) C4–C7	Antibonding (σ*)	0.01133	6.98	0.81	0.052

The NBO study of this compound shows significant donor–acceptor interactions, specifically lone pairs from oxygen and nitrogen atoms donating into neighboring bonds' antibonding orbitals. The LP(2) on oxygen O19 donates to the π* antibonding orbital of C13–C15 with a stabilization energy of 19.76 kcal/mol, causing significant delocalization. This shows the molecule's effective electron density redistribution and strong electronic polarizability. Significant lone pair interactions between atoms, such as N6 and O17, and nearby σ* antibonding orbitals suggest substantial electron-donating capabilities, particularly via heteroatoms, which are essential for metal surface adsorption. Electron density donation improves coordination with metal d-orbitals, enabling surface chemisorption.

Molecular stability and adsorption are enhanced by substantial intramolecular charge delocalization, as shown by considerable stabilization energies ($E^2 > 10$ kcal/mol in numerous contacts). Donor-acceptor transitions enhance the molecule's affinity for metal-inhibitor complexes, particularly through lone-pair-rich centers such as oxygen and nitrogen, which are well-suited for interacting with Fe^{2+}, Cu^{2+}, or Zn^{2+} in corrosion systems. Overall, the NBO investigation confirms the molecule's effectiveness as a corrosion inhibitor. The donor–acceptor interactions, particularly those involving lone pairs and antibonding orbitals, exhibit significant potential for electron donation and charge delocalization, enabling effective adsorption and the creation of protective layers on metal surfaces to prevent corrosion.

3. Study of corrosion by weight loss

The weight loss method was employed to investigate the corrosion inhibition performance of two synthesized derivatives, M1 and M2, on mild steel in an acidic medium over 24 hours at room temperature. The results indicate a clear concentration-dependent inhibition behavior for both derivatives. For M2, the highest concentration (1×10^{-2} M) demonstrated a remarkable corrosion rate reduction to 0.0536 $mg\cdot cm^{-2}\cdot h^{-1}$ with an inhibition efficiency (IE%) of 96.0% and surface coverage (θ) of 0.96. This suggests that M2 forms a highly protective barrier layer on the metal surface, significantly hindering corrosive attack. Similarly, M1 exhibited a strong inhibitory effect at the same concentration, achieving 94.52% IE% and θ = 0.9452, although it was slightly less effective than M2. As the concentration of both inhibitors decreased, corrosion rates increased, and both IE% and θ declined, confirming the dose-dependent inhibition pattern typical of adsorptive organic inhibitors, as shown in Tables 7 and 8.

The calculated Gibbs free energy of adsorption ($\Delta G^0_a d_s$) further supports the spontaneous and physical nature of adsorption for both M1 and M2. The most negative value observed for M2 was –22.73 kJ/mol at the lowest tested concentration, while for M1, the maximum $\Delta G^0_a d_s$ was –22.29 kJ/mol. These values fall within the range associated with physisorption (–20 to –40 kJ/mol), suggesting that the inhibitor molecules interact with the mild steel surface predominantly through electrostatic forces rather than covalent bonding. The slightly more negative $\Delta G^0_a d_s$ values for M2 compared to M1 align with its superior inhibition efficiency. Overall, both compounds act as effective corrosion inhibitors, with M2 showing marginally better performance, likely due to more favorable molecular orientation or electron-donating functional groups that enhance surface adsorption. These findings highlight the practical potential of these derivatives in mitigating acid-induced corrosion in industrial settings.

Table 7. Corrosion Inhibition Parameters of M1 Derivative on Mild Steel in Acidic Medium: Weight Loss Assessment at Room Temperature

Dosage of (Mild steel)	Rate of corrosion	Φ	IE percentage	ΔG^o_{ads}
M1				
1×10^{-2}	0.0373	0.9747	97.4714	-38.53
5×10^{-3}	0.0785	0.9439	94.3979	
1×10^{-3}	0.1756	0.8715	87.1544	
5×10^{-4}	0.2465	0.8286	82.8653	

Table 8. Corrosion Inhibition Parameters of M2 Derivative on Mild Steel in Acidic Medium: Weight Loss Assessment at Room Temperature.

Dosage of (Mild steel)	Rate of corrosion	Φ	IE percentage	ΔG^{o}_{ads}
M2				
1×10^{-2}	0.0372	0.9747	97.4713	-38.13
5×10^{-3}	0.0784	0.9439	94.3978	
1×10^{-3}	0.1757	0.8515	85.1545	
5×10^{-4}	0.2967	0.7986	79.8655	

Note: The corrosion rate ($mg.cm^{-2}.h^{-1}$) of the blank is 1.3403, and the unit of ΔG^{o}_{ads} is ($kJ.\ mol^{-1}$).

This study presents a valuable advancement in corrosion mitigation strategies for petroleum infrastructure, particularly storage tanks and pipelines, is exposed to acidic environments. The synthesized Mannich base derivatives (M1 and M2) demonstrated high inhibition efficiencies (above 97%) at low concentrations, forming robust protective layers on mild steel surfaces. The negative values of Gibbs free energy (ΔG^{o}_ads ≈ –38 kJ/mol) confirm the spontaneous physisorption mechanism, enabling a reliable physical barrier that reduces metal interaction with corrosive species such as H^{+} and Cl^{-} ions.

In practical oilfield applications, these inhibitors can be injected into acidic crude oil pipelines or used in tank preservation systems to prevent internal corrosion, eliminating the need for costly alloy upgrades or continuous maintenance. The presence of electron-donating groups, such as hydroxyl and amine functionalities, enhances surface affinity, ensuring strong yet reversible adsorption under fluctuating temperature and pH conditions. Furthermore, the DFT-based design and validation of these molecules enable the precise tuning of their electronic properties, allowing engineers to develop next-generation, environmentally safe corrosion inhibitors tailored to specific field conditions. As a result, this research supports more cost-efficient, scalable, and eco-friendly corrosion control strategies in petroleum operations.

Conclusion

In conclusion, this study successfully demonstrates the synthesis, characterization, and corrosion inhibition evaluation of two novel Mannich base derivatives (M1 and M2) for mild steel protection in acidic environments. Both compounds exhibited excellent inhibition efficiencies above 97% at a concentration of 1×10^{-2} M, primarily through spontaneous physisorption mechanisms, as supported by $\Delta G^{o}_{a}d_{s}$ values and surface coverage analysis. The functional groups, such as hydroxyl and amino moieties, significantly contributed to the adsorption strength on the steel surface. Moreover, DFT-based simulations provided insights into the electron-donating nature and molecular stability of these inhibitors, highlighting their potential for forming uniform and adherent protective layers. Because corrosion remains a major challenge in oil and gas infrastructure, adopting such low-cost, effective, and environmentally benign inhibitors represents a strategic advancement. Additionally, since both

inhibitors performed efficiently at relatively low concentrations, they are suitable for practical field applications. However, although this study confirms high inhibitory performance under laboratory conditions, real-world systems present fluctuating parameters such as temperature, pressure, and salinity. Therefore, we will complete the other applications by conducting long-term field tests, synergistic evaluations with other green additives, and further structure–activity relationship (SAR) optimizations. Furthermore, future research should explore nanocarrier systems or inhibitor coatings for sustained release, aiming for comprehensive protection in harsh industrial conditions. If such improvements are achieved, these inhibitors can form the basis of next-generation corrosion control agents aligned with environmental and operational standards.

References

1. Assad H, Lone IA, Sharma PK, Kumar A. Corrosion in the Oil and Gas Industry. Industrial Corrosion: Fundamentals, Failure, Analysis and Prevention. 2025:39-63.
2. Bender R, Féron D, Mills D, Ritter S, Bäßler R, Bettge D, et al. Corrosion challenges towards a sustainable society. Materials and corrosion. 2022;73(11):1730-51.
3. Amaya-Gómez R, Bastidas-Arteaga E, Sánchez-Silva M, Schoefs F, Muñoz F. Corrosion and Reliability Assessment of Inspected Pipelines: Springer; 2023.
4. Eliyan FF. Imidazoline Inhibitors for Corrosion Protection of Oil Pipeline Steels: Experimental Laboratory Evaluation and Case Studies: John Wiley & Sons; 2024.
5. Jawad AA, Jber NR, Rasool BS, Abbas AK. Tetrazole derivatives and role of tetrazole in medicinal chemistry: An article review. Al-Nahrain Journal of Science. 2023;26(1):1-7.
6. Shah BA, Muthalif AG. A comprehensive review on corrosion management in oil and gas pipeline: methods and technologies for corrosion prevention, inspection and monitoring. Anti-Corrosion Methods and Materials. 2025.
7. Verma C, Ebenso EE, Quraishi M, Hussain CM. Recent developments in sustainable corrosion inhibitors: design, performance and industrial scale applications. Materials Advances. 2021;2(12):3806-50.
8. Al-Amiery AA, Al-Azzawi WK. Mannich bases as corrosion inhibitors: An extensive review. Journal of Molecular Structure. 2023;1294:136421.
9. Sharma S, Ganjoo R, Thakur A, Kumar A. Electrochemical characterization and surface morphology techniques for corrosion inhibition—a review. Chemical Engineering Communications. 2023;210(3):412-47.
10. Aslam R, Mobin M, Zehra S, Aslam J. A comprehensive review of corrosion inhibitors employed to mitigate stainless steel corrosion in different environments. Journal of Molecular Liquids. 2022;364:119992.
11. Tokalı FS, Taslimi P, Demircioğlu İH, Şendil K, Tuzun B, Gülçin İ. Novel phenolic Mannich base derivatives: synthesis, bioactivity, molecular docking, and ADME-Tox Studies. Journal of the Iranian Chemical Society. 2022;19(2):563-77.
12. Singh P, Harbola MK. Density-functional theory of material design: fundamentals and applications-I. Oxford open materials science. 2021;1(1):itab018.

13. Abu Radia M, Saafan SA. An Overview for Beginners on Density Functional Theory in Computational Materials Science and Some of the Related Software Packages. Egyptian Journal of Solids. 2025;47(1):110-38.
14. Aziz I, Abdulkareem M, Annon I, Hanoon M, Alkaabi M, Shaker L, et al. Corrosion inhibition potential of a new corrosion inhibitor for mild steel in 1 M hydrochloric acid solution determined by weight loss technique, complemented with adsorption studies and DFT calculations. Int J Corros Scale Inhib. 2022;11(1):64.
15. Ali ZH, Saleem D, Abbas AK, Rasool BS, Cheyad MS. Synthesis and estimation of the insecticide and antibacterial activities for some new amide derivatives. Indonesian Journal of Chemistry. 2023;23(6):1535-41.
16. Abbas AK, Jber NR. Synthesis and Characterization of New Oxazepine Compounds and Estimation its Biological Activity. Al-Nahrain Journal of Science. 2020;23(3):17-23.
17. Hameed MA, Al-Jeboori MJ. Synthesis, spectral characterisation, DFT calculations, biological evaluation and molecular docking analysis of new Mannich compounds derived from cyclopentanone. Journal of Molecular Structure. 2025;1322:140619.
18. Abeng F, Nyong B, Ikpi M, Obeten M. The role of computational chemistry in corrosion inhibition: a review. Port Electrochim Acta. 2022;40(4):243-58.
19. Bakheit AH, Alkahtani HM. Integrated structural, functional, and ADMET analysis of 2-methoxy-4, 6-diphenylnicotinonitrile: the convergence of X-ray diffraction, molecular docking, dynamic simulations, and advanced computational insights. Molecules. 2023;28(19):6859.
20. Farag AA, Tawfik SM, Abd-Elaal AA, Abdelshafi N. Detailed DFT/MD simulation, QSAR modeling, electrochemical, and surface morphological studies of self-assembled surfactants as eco-friendly corrosion inhibitors for copper in 1 M HNO3 solution. Journal of Industrial and Engineering Chemistry. 2024;138:237-55.
21. Zhang Y, Sheong FK, Lin Z. Natural Fragment Bond Orbital Method for Interfragment Bonding Interaction Analysis. Journal of the American Chemical Society. 2024;146(50):34591-9.

Web of Scientists and Scholars: Journal of Multidisciplinary Research